JOURNAL OF PROPULSION AND POWER
Vol. 9, No. 4, July–Aug. 1993

Modeling Supersonic Inlet Boundary-Layer Bleed Roughness

Gerald C. Paynter,* David A. Treiber,† and W. David Kneeling‡
The Boeing Company, Seattle, Washington 98124

Boundary-layer mass removal (bleed) through spanwise bands of holes on a surface is used to prevent or control separation in supersonic inlets. The rough wall algebraic turbulence model of Cebeci and Chang was added to both boundary-layer and Navier-Stokes analyses to simulate the overall effect of bleed on the growth of a boundary layer. Roughness values were determined for seven bleed configurations, a range of Mach numbers between 1.3–4, and bleed rates between zero and choked values. For the bleed experiments considered, the roughness was found to be a function of the fraction of the upstream boundary-layer mass flux removed. Choked bleed flow through holes at a low angle, with respect to the surface, minimized the roughness effect and gave the best improvement in the boundary-layer velocity distribution for separation control.

Nomenclature

A^+ = Van Driest parameter, 26
d = bleed hole diameter
k = von Karman constant, 0.4
k_s = equivalent sand grain roughness
L/d = hole aspect ratio
l = local turbulent length scale
M = Mach number
N = number of rows of bleed holes in bleed band
p/p_∞ = local static pressure/freestream static pressure
R = roughness parameter, in.
u/u_e = ratio of local to freestream velocity within the boundary layer
u_τ = $(\tau_w/\rho_w)^{1/2}$
u' = local turbulent velocity scale
w_{bl} = boundary-layer mass flux below y where $u/u_e = 0.99$
w_{bleed} = bleed rate
X/d = streamwise spacing of bleed holes
Y/d = cross stream spacing of bleed holes
y = distance normal to the wall
y^+ = yu_τ/ν_w
α = bleed hole angle to surface
δ = boundary-layer thickness
μ_t = turbulent viscosity
ν_w = kinematic viscosity at the wall
ρ = density
ρ_w = density at the wall
τ_w = wall shear stress

Introduction

THERE is increased interest in the use of Navier-Stokes (NS) analysis for inlet design support, because such analysis is now feasible due to increases in computer memory and speed. Since boundary-layer mass removal or bleed on an inlet wall is used for boundary-layer control, bleed effects must be included in the simulations. While it is possible to predict the flow through individual bleed holes with NS analysis, this is impractical in the context of an inlet design because of the size and complexity of the grid that would be required. If NS analyses are to be useful for inlet design, a simulation of the effect of bleed on the boundary layer is needed that does not require a local grid adequate to resolve the flow through each hole. The bleed simulation model should relate changes in the boundary-layer velocity distribution across a bleed band to the bleed hole configuration, bleed flow rate, and local freestream Mach number without increasing the grid required to resolve the boundary layer. The purpose of this article is to propose an algebraic turbulence model modified to include the overall effect of bleed for use in NS simulations of inlet flows. Results derived from boundary-layer and NS analysis of several experiments are reported for seven bleed configurations tested over a range of freestream Mach numbers.

A typical bleed band[1,2] (Fig. 1) might consist of four rows of circular holes either at an angle or normal to the surface. Bleed can affect the aircraft flow in three ways: 1) inlet boundary-layer velocity profile improvement; 2) increased drag; and 3) increased mixing in the boundary layer in the bleed region and for some distance downstream. Of the three effects, the increased drag and increased mixing are detrimental. It is possible to bleed a substantial amount of flow from the boundary layer and achieve a net performance loss, because the increased mixing from a particular configuration and the drag overwhelm the beneficial effect associated with removal of the low-momentum near-wall flow.

Linear and semilog plots of velocity distributions in a turbulent boundary layer are sketched in Fig. 2. The figure shows the individual effects of mass removal, mixing, and adverse pressure gradient on the boundary-layer velocity distribution relative to a smooth flat plate boundary layer. Note that the adverse gradient and mixing effects reduce the velocity at a given distance from the wall, and that bleed (idealized bleed through a smooth porous surface) increases the velocity relative to a smooth wall velocity distribution. The process of bleed through individual holes, like surface roughness, increases mixing which reduces the desired increase in u/u_e. The local reduction of velocity due to the increase in near-wall mixing with bleed is the "bleed roughness effect."

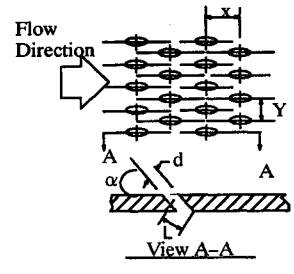

Fig. 1 Typical bleed band configuration.

Received April 27, 1992; revision received March 15, 1993; accepted for publication March 17, 1993.

*Associate Technical Fellow. Associate Fellow AIAA.
†Senior Specialist Engineer.
‡Senior Engineer.

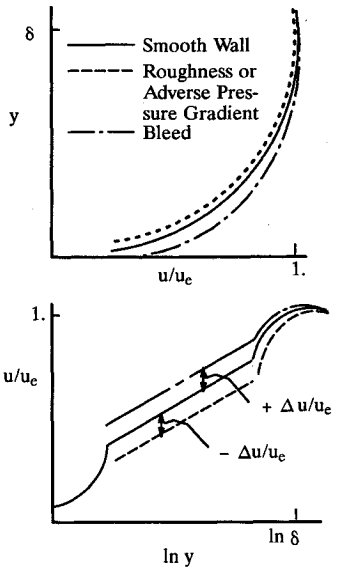

Fig. 2 Adverse pressure gradient, roughness, and bleed effects on the boundary layer.

The physical mechanism responsible for bleed roughness is not well understood. The failure of smooth wall turbulence modeling to predict this effect accurately was noted nearly 20 yr ago.[3] However, bleed roughness is not always observed.[4] The magnitude of the effect appears to depend on the bleed geometry, local flow conditions, and bleed flow rate. Roughness is a good analogy for inlet bleed, because air enters the holes with a streamwise component of momentum and emerges with none.[5] Since bleed through an individual hole should result in time-averaged trailing vortices, it is reasonable to expect these vortices to further increase the mixing, and therefore the effective roughness of a surface, although other flow processes such as a local flow instability associated with an individual hole could be responsible for the effect.

Approach

Bleed roughness was simulated using the algebraic turbulence model of Cebeci-Chang.[6] The near-wall length scale distribution was modified to include the effects of surface roughness as suggested by Rotta,[7] through addition of a constant defined as a roughness parameter. A relationship was developed between the increase in the near-wall length scale and an equivalent sand grain roughness Reynolds number valid over a wide range of roughness values. The model was implemented in the boundary-layer method of Reyhner[8] (through a modification of the Cebeci-Smith model), and in the NS analysis (through a modification of the Baldwin-Lomax model). In the near-wall region, the two models are identical. Roughness values were determined for selected experiments by varying the roughness value input to either analysis until a match was obtained between the computed and measured near-wall velocity distributions at a station just downstream of the bleed band. (Bleed is known to decrease the near-wall length scale. Consequently, the roughness parameter actually includes the combined effects of both bleed and roughness.) The expansion induced by the bleed flow and the recompression shock downstream of the bleed band were neglected in the boundary-layer analysis but included in the NS analysis. The bleed rate and roughness were assumed to be constant over the streamwise extent of the bleed region. The roughness was set to zero downstream of the bleed region.

Roughness values were determined for seven bleed configurations, a range of Mach numbers between 1.3–4, and bleed rates between zero and choked bleed hole values. Although bleed is used in an inlet both upstream of, and within, regions of adverse pressure gradient, it was thought important to separate the effects of pressure gradient and bleed roughness. Consequently, the pressure gradient was negligible for most of the cases selected. Several cases were selected, however, where bleed was used in the region of a shock/boundary-layer interaction.

Comparisons were made between NS results and the boundary-layer method results to establish that the roughness model implemented in the NS analysis would produce the same changes in boundary-layer properties across a bleed region as the boundary-layer method. The NS code was then applied to several shock boundary-layer interactions with bleed in the region of interaction to investigate the effect of a strong adverse pressure gradient on the bleed roughness.

In the mixing length hypothesis, the turbulent viscosity is assumed to be

$$\mu_t = \rho l u'$$

For a smooth wall, in the near-wall region, the velocity scale is

$$u' = l \left| \frac{du}{dy} \right|$$

The length scale is assumed to be

$$l = ky[1 - \exp(-y^+/A^+)]$$

For a rough wall, the Cebeci-Chang model assumes the length scale in the near-wall region is

$$l = k(y + R)\{1 - \exp[-(y + R)^+/A^+]\}$$

The equivalent sand grain roughness can be computed from the roughness constant using an empirical relationship[9]:

$$k_s = R/0.031$$

Experiments

Cases were selected to explore a range of Mach numbers and configurations. No attempt was made to establish roughness values for all of the available boundary-layer bleed experiments. Most selected cases had no streamwise pressure gradient, and a roughness value could be established using the boundary-layer analysis. A few cases were selected to explore the combined effects of bleed and an adverse pressure gradient. For these, bleed was used in the region of a shock/boundary-layer interaction, and the NS analysis was used to establish a roughness.

While a comprehensive review of all of the available boundary-layer bleed data was not attempted, data cases were selected that satisfied the following criteria:

1) The bleed geometry was well-described in the research article and included the number of holes, spacing, pattern, angle, diameter, porosity, and the length-to-diameter ratio.

2) The freestream Mach number distribution across the bleed region was available.

3) The freestream Reynolds number and the local wall temperature were available.

4) The bleed mass flux was available.

5) Boundary-layer velocity distributions were available both upstream and downstream of the bleed region.

In the selected experiments, freestream Mach numbers ranged between 1.3–4. Bleed geometries consisted of staggered rows of holes at angles relative to the surface between 20–90 deg, and one porous wall configuration as illustrated in Fig. 3. Bleed rates ranged between zero and choked flow. The wall temperature for both experiments was approximately adiabatic.

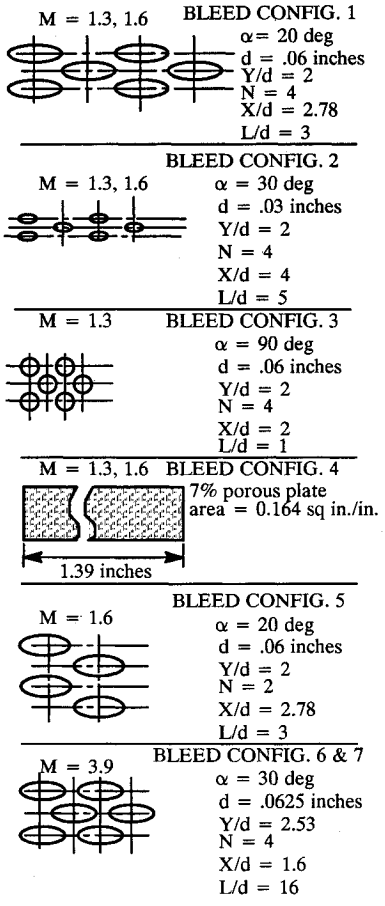

Fig. 3 Bleed configurations.

Schuehle Experiment

In the Schuehle[10] experiment, Fig. 4, the Mach number, boundary-layer properties over the test surface, and the bleed geometry could be varied. The bleed hole size and pattern were varied by using removable inserts with bleed perforations. The Mach number over the test surface was varied by rotation of the model to change the strength of the shock at the test surface leading edge. The boundary-layer properties on the test surface were varied by translating the rectangular test section of the model up and down to scoop more or less of the tunnel wall boundary layer onto the test surface.

The model had two profile measuring stations on the test surface. The upstream station was 3-in. aft of the test surface leading edge, and the downstream profile station was 5-in. aft of the leading edge (measured along the plate). The flow through the bleed band was measured with a metering device in the duct from the bleed plenum.

Configurations 1–5 were tested at local freestream Mach numbers of 1.3 and 1.6. The bleed hole diameter and the hole angle to the surface were varied in the configurations tested. The streamwise extent of the bleed regions was between 0.3–1.4 in. The boundary layer upstream of the bleed region was fully developed. The displacement thickness was varied between 0.03–0.06 in., and the boundary-layer thickness varied between 0.24–0.38 in., depending on the portion of the tunnel wall boundary layer scooped onto the test surface.

While the range of flow conditions and geometries investigated by Schuehle were the most extensive of the experiments considered, the experiment had two potential problems. First, scooping a portion of the tunnel boundary layer onto the test surface with only 3 in. (about 10 boundary-layer thicknesses) for redevelopment may have produced a nonequilibrium boundary layer at the bleed region. The scale of turbulence in the outer part of the layer may have been characteristic of the thick tunnel wall boundary layer from which

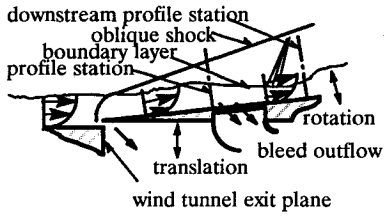

Fig. 4 Schuehle experiment.

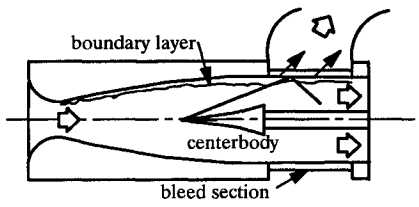

Fig. 5 Mayer experiment.

it originated.[11] Second, the shock originating near the plate leading edge (used to change the Mach number over the test surface) may have introduced a nonuniformity in the mean velocity distribution. Because the Mach number was low supersonic at the leading edge of the test surface, the shock at the leading edge was detached and changed in strength as a function of distance away from the surface. The variation in shock strength caused a variation in total pressure through the boundary layer and may have distorted the mean velocity distribution through the boundary layer on the test surface.[12]

Mayer Experiment

In the Mayer[13] experiment (Fig. 5), the test surface was the outer wall of an axisymmetric wind tunnel 3.0-in. in diameter. The bleed band was 0.425-in. in streamwise extent, the upstream measuring station was 0.75-in. forward of the bleed band, and the downstream measuring station was 1.5-in. downstream of the bleed band. A contoured centerbody was used to generate a distributed compression on the outer wall in the bleed region. Boundary-layer surveys were taken at 15 measuring stations spaced along the surface including the upstream and downstream measuring stations. With zero bleed flow, a rubber seal was placed over the bleed holes within the bleed plenum to prevent any local flow through the holes due to recirculation within the bleed plenum. The boundary-layer thickness upstream of the bleed band was about 0.25 in., and the displacement thickness was about 0.09 in. A number of flow conditions were investigated including zero and choked hole bleed flow rates both with and without adverse pressure gradient. Configurations 6 and 7 in Fig. 3, consisting of four rows of 0.0625-in.-diam 30-deg slanted holes, were tested at a local freestream Mach number of 3.9. For configuration 6, the centerbody was positioned to place the adverse pressure gradient downstream of the aft profile measurement station. For configuration 7, the adverse gradient was positioned over the bleed band.

Results and Discussion

The effects of bleed and roughness on a boundary layer developing over a bleed band are illustrated for bleed configurations 1 and 2 from the Schuehle experiment at a local freestream Mach number of 1.6. The boundary-layer velocity distributions at the downstream profile measuring station are compared in Fig. 6. Note that for configuration 1, all of the velocity profiles are less full than the smooth wall profile, except the case where w_{bleed} = 0.078 lb/s (choked). For configuration 2, the hole diameter is half that of configuration 1, and only the zero bleed profile is less full than the smooth wall profile. The figure illustrates the effects of bleed rate and roughness as a function of hole diameter. The larger holes

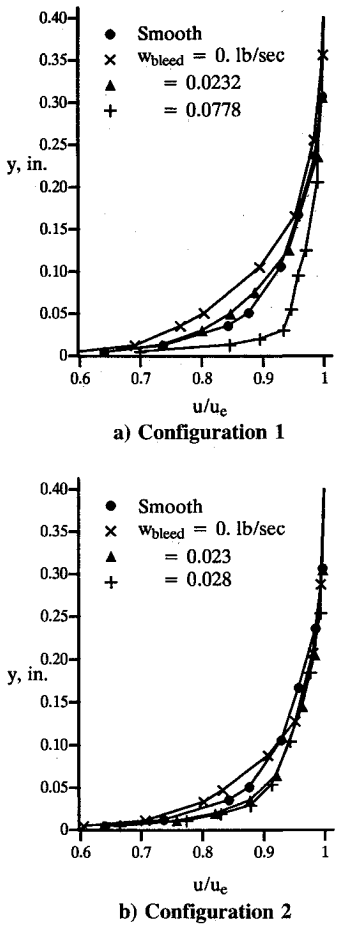

Fig. 6 Bleed and roughness effects at M = 1.6.

of configuration 1 allow more mass to be removed at the choked bleed rate, and this results in more profile improvement than configuration 2.

The roughness for a given configuration was determined by initializing the boundary-layer or NS analysis at the upstream profile measuring station using the measured boundary-layer velocity distribution (assuming an equilibrium turbulent boundary layer), computing the boundary-layer development over the bleed band to a measuring station downstream of the bleed band for a range of roughness values, and then selecting a roughness value that gave a match between the predicted and measured velocity profiles at the downstream measuring station in the near-wall region. The match was determined from semilog plots of the predicted and measured profiles (similar to those shown in Fig. 2). Predicted and measured profiles were matched at 10% of the upstream boundary-layer thickness from the wall. Roughness values determined through this matching procedure were found to be insensitive to the distance from the wall where the match was obtained because of the linear nature of the velocity profiles in the near wall region on a semilog plot. The bleed and the roughness were assumed to be uniform over the bleed band. In a preliminary study with the boundary-layer analysis, the computed roughness for a given configuration and flow condition was found to be insensitive to the streamwise distribution of bleed across the bleed band. For the boundary-layer analysis, a constant wall temperature boundary condition and a turbulent Prandtl number of 1 were used. For the NS analysis, an adiabatic wall temperature boundary condition and a turbulent Prandtl number of 0.9 were used.

Bleed causes a near-wall shift in u/u_e relative to a smooth plate velocity distribution. This shift is a measure of the ability of the boundary layer to traverse a region of adverse pressure gradient without separation. The near wall shifts in u/u_e at the downstream measurement station for configurations 1–5 were compared at the choked bleed rate. The choked bleed rate for each configuration is unique to that configuration, and is a function of the hole diameter and angle. The shift in u/u_e was determined at a distance of 10% of the upstream boundary-layer thickness from the wall (still within the log law region). Configuration 1 provided the most improvement in the near-wall velocity distribution at both Mach 1.3 and 1.6 because the discharge coefficient of the slanted holes is substantially better than that for the normal holes; the open area of configuration 1 is equal to that of configurations 3 and 4. The velocity profile improvement was a strong function of the bleed rate for these five bleed configurations.

Boundary-Layer Analysis Results

The roughness parameter as a function of the bleed rate referenced to the upstream boundary-layer mass flux is plotted in Fig. 7 for the angled hole configurations 1, 2, and 5. Roughness values for all of the configurations ranged between 0–0.001 in. at zero bleed. Most configurations were tested with two boundary-layer thicknesses over the test surface. This resulted in the scatter in roughness shown in the figure. For configuration 1, when there was bleed—but the holes were unchoked, the roughness was found to vary between 0.0015–0.0025 in. For a choked bleed rate, the roughness was found to vary between 0–0.0005 in. The negligible roughness with slanted bleed holes when choked was unexpected.

A second unexpected trend was found for configuration 2; whether the roughness was a strong function of the bleed rate or not seemed to depend on the relative thickness of the initial boundary layer. With a thick initial boundary layer, the roughness was found to range between 0–0.0005 in. for bleed values between zero and choked; the bleed rate had little effect on the roughness. With a thin initial boundary layer, the roughness at an unchoked bleed rate was similar to that of configuration 1; the roughness was significant and a strong function of the bleed rate.

The roughness parameter for configuration 3 (90-deg holes) (Fig. 8) was found to be zero, except at the choked bleed rate where it ranged between 0–0.002 in. The trends of low roughness for the 90-deg holes at unchoked bleed rates and high roughness when choked, are inconsistent with the trends for the angled hole configurations. For configuration 4 (a porous surface), the roughness was found to increase with the bleed rate with a maximum value of 0.002 in. at the choked bleed rate.

The roughness results can be summarized as follows for all of the configurations considered. For bleed rates up to about 3% of the upstream boundary-layer mass flux, bleed has little effect (other than the mass removal) on the boundary-layer development and the roughness is insignificant. Between bleed rates of 3–15%, bleed has a strong effect on the boundary-

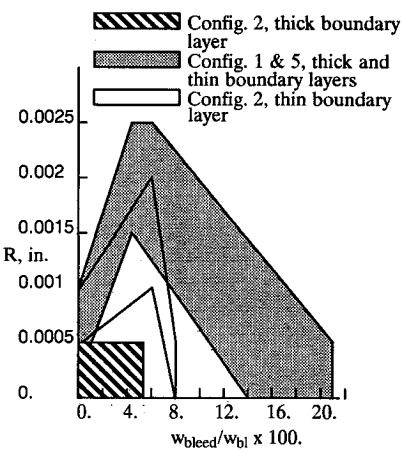

Fig. 7 Roughness for configurations 1, 2, and 5.

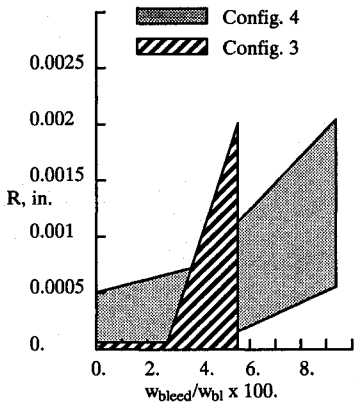

Fig. 8 Roughness for configurations 3 and 4.

layer development and the roughness is important. Above a bleed rate of about 15% of the boundary-layer mass flux, the boundary-layer growth rate is unaffected by the bleed (except for the mass removal) and the roughness is insignificant. A bleed rate of 12–15% of the upstream boundary-layer mass flux represents removal of the log law portion of the upstream boundary layer. It may be that while the disturbances due to the bleed holes are still present, removal of the log law region brings the large scale wake region turbulence in contact with the wall and that this would then become the dominant mixing mechanism.

For all configurations except the porous wall, the peak roughness can be related to the hole diameter through the empirical relationship between sand grain roughness and the roughness parameter. Using this expression, the maximum equivalent sand grain roughness for a configuration is approximately equal to the bleed hole diameter.

NS Analysis Results

The NS code used for the bleed study was PARC,[14] a version of the NASA-Ames code ARC2D.[15] Implementation of the bleed roughness model in the code was straightforward. The Baldwin-Lomax turbulence model[16] was modified in the near-wall layer in the same way as the Cebeci-Smith model of the boundary-layer analysis method. Both methods use identical formulations of the near-wall length scale. The imposition of bleed at the wall in the code was done by specifying a uniform normal mass flux along the wall encompassed by the bleed holes, and extrapolating density and pressure.

Figure 9 shows a Mach contour plot of the computed flowfield for configuration 7. 7.2% bleed was imposed and, over the bleed band, a smooth wall was assumed. The effect of the compression produced by the centerbody can be seen as a slight thickening of the boundary layer just upstream of the bleed region. The computational grid in the downstream part of the channel had 151 uniformly spaced points in the streamwise direction ($\Delta x = 0.02$ in.) and 50 points in the cross stream direction, tightly spaced on one side to resolve the wall boundary layer. The bleed band is covered by 16 streamwise points. The inflow plane of the constant area channel segment was initialized with the boundary-layer profile from the first experimentally measured station. For runs with the centerbody present, an Euler solution consisting only of the centerbody was computed using a 212 × 50 mesh. The outflow boundary flowfield of that solution was then superimposed on the measured boundary-layer profile and used as the inflow condition of the constant area bleed section.

Figure 10 compares the computed and experimentally measured boundary-layer profiles downstream of the bleed band for the case of 3.8% bleed without the pressure interaction present (configuration 6). The rough wall computation used a roughness factor of $R = 0.006$ in., which was found from the data correlation using the boundary-layer analysis program. The calculation correctly predicts the increased turbulent mixing in the near-wall region, while at the same time removing the correct amount of mass from the duct. In Fig. 11, the wall static pressures from the calculations assuming smooth and rough walls are compared to test data. The strengths of the predicted local expansion and compression at the leading and trailing edges of the bleed band are decreased with surface roughness, and this improves agreement with the pressure measured in the bleed region.

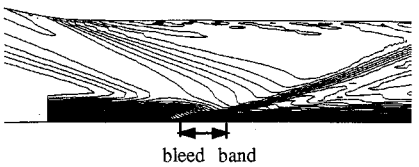

Fig. 9 Mach number contours for configuration 7.

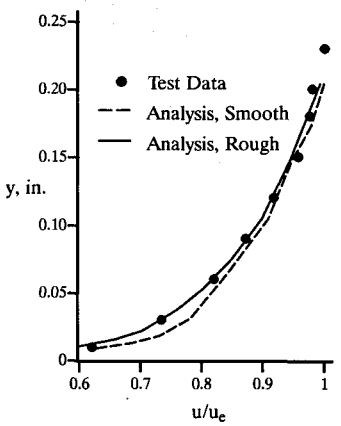

Fig. 10 Boundary-layer profiles for configuration 6.

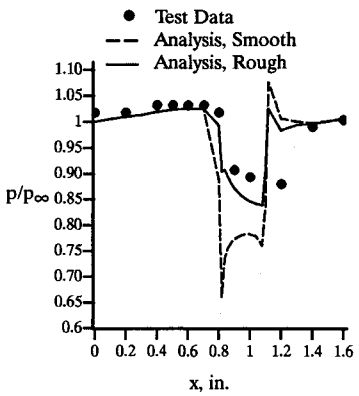

Fig. 11 Wall static pressure distribution for configuration 6.

The final case is 7.2% bleed in the presence of the pressure rise over the bleed band. The calculation correctly predicts fully attached flow as a result of the bleed. The downstream velocity profile (Fig. 12) is not accurately predicted, even when the bleed roughness factor arrived at from the 3.8% bleed zero adverse pressure gradient case is used in the prediction. A higher value of roughness would have been required to obtain a good match between predicted and measured boundary-layer velocity profiles at stations downstream of the bleed band.

The results for this 7.2% bleed case are qualitatively consistent with the results from the Schuehle experiment. Although the bleed holes were choked in both the 3.8 and the 7.2% bleed cases (for the same geometry), more bleed is removed with the adverse pressure gradient over the bleed band because of the higher local static pressure on the bleed surface. At 7.2% bleed, more of the log-law part of the boundary layer is brought into contact with the surface, and the

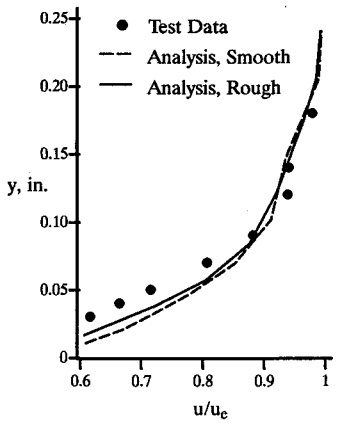

Fig. 12 Boundary-layer profiles for configuration 7 with pressure interaction.

bleed roughness should be higher than for the 3.8% bleed case to be consistent with roughness values derived from the Schuehle experiment.

Mesh refinement studies were performed on selected runs. Initially, a near-wall normal grid spacing of 0.001 in. was selected, which yielded a $y^+ = 2$ for the converged boundary layer, which is within the viscous sublayer. The mesh was refined to 0.0001 in. ($y^+ = 0.2$), and convergence was slowed slightly for the cases without bleed, but the results showed no plottable difference. For the cases with bleed, the refined spacing was used because of rapid boundary-layer thinning over the bleed band. This caused all the coarse mesh points to be in a supersonic region of the boundary layer. As a result, the bleed boundary condition was ill-posed, and convergence was slowed. With the refined mesh, the first five points away from the bleed band were subsonic, and good convergence was achieved.

Conclusions

The algebraic turbulence model of Cebeci and Chang provides an adequate description of the boundary-layer development over, and downstream, of a bleed region in a supersonic turbulent boundary layer. The model is capable of predicting the overall increased mixing effect that may result from mass removal through a band of discrete bleed holes.

The roughness of a given bleed configuration was found to be a function of the hole diameter, hole angle, and bleed rate. The roughness was almost independent of Mach number for the Schuehle configurations tested at Mach numbers of 1.3 and 1.6. The roughness of the angled hole configurations was found to be zero when 12–15% of the upstream boundary layer was removed with bleed.

For the same open area in a bleed band, the choked bleed mass flux through 90-deg bleed holes was only about one-fourth that obtained through low-angled holes. Low-angled bleed holes were found to be more effective than 90-deg holes in increasing u/u_e in the near-wall region. An increase in u/u_e in the near-wall region should increase the adverse pressure gradient required to separate the boundary layer. The current study suggests that inlet bleed configurations with holes at low angle (20 or 30 deg) to a surface are more effective for preventing or delaying separation than configurations with 90-deg holes or a porous surface material for a given bleed flow rate.

For the bleed experiments considered, the roughness was found to be a function of the fraction of the upstream boundary-layer mass flux removed with bleed. Up to a bleed rate of about 3% of the upstream boundary layer mass flux, the boundary-layer growth rate was relatively unaffected (except for the mass removal). At bleed rates between 3% and 12–15%, the boundary-layer growth rate was strongly affected. Above a bleed rate of 15% the growth rate was relatively unaffected.

References

[1]Paynter, G. C., and Chen, H. C., "Progress Toward the Analysis of Supersonic Inlet Flows," AIAA Paper 83-1371, June 1983.

[2]Syberg, J., and Hickcox, T. E., "Design of a Bleed System for a Mach 3.5 Inlet," NASA CR-2187, Sept. 1972.

[3]Reyhner, T. A., and Hickcox, T. E., "Combined Viscous-Inviscid Analysis of Supersonic Inlet Flowfields," *Journal of Aircraft*, Vol. 9, No. 8, 1972, pp. 589–595.

[4]Hamed, A., and Shang, J., "Survey and Assessment of Validation Data Base for Shockwave Boundary Layer Interactions in Supersonic Inlets," AIAA Paper 89-2939, July 1989.

[5]Bradshaw, P., private communication, Mechanical Engineering Dept., Stanford Univ., Stanford, CA, June 11, 1990.

[6]Cebeci, T., and Chang, K. C., "Calculation of Incompressible Rough-Wall Boundary Layer Flows," *AIAA Journal*, Vol. 16, No. 7, 1978, pp. 730, 731.

[7]Rotta, J. C., "Turbulent Boundary Layers in Incompressible Flow," *Progress in Aerospace Science*, Vol. 2, 1962, pp. 1–219.

[8]Reyhner, T. A., "A Computer Program for Finite-Difference Calculation of Compressible Turbulent Boundary Layers," Boeing Document D6-23236, Seattle, WA, June 1970.

[9]Kays, W. M., and Crawford, M. E., "Convective Heat and Mass Transfer," 2nd ed., McGraw-Hill, New York, 1980, p. 187.

[10]Schuehle, A. L., "Tabulation of the Boundary Layer Profile Data Taken for the SST Bleed System Development and Performance Test," Boeing Mechanical Engineering TM-70-50, Aug. 26, 1970.

[11]Harloff, G., private communication, Sverdrup Technology, Inc., Middleburg Heights, OH, May 1990.

[12]Bradshaw, P., private communication, Mechanical Engineering Dept., Stanford Univ., Stanford, CA, April 3, 1990.

[13]Mayer, D. W., "Turbulent Supersonic Boundary Layer Flow in an Adverse Pressure Gradient Including the Effects of Mass Bleed," M.S. Thesis, Univ. of Washington, Seattle, WA, 1977.

[14]Cooper, G. K., "The PARC Code: Theory and Usage," Arnold Engineering Development Center TR-87-24, Arnold Air Force Base, TN, Oct. 1987.

[15]Pulliam, T. H., "Euler and Thin Layer Navier-Stokes Codes: ARC2D, ARC3D," Computational Fluid Dynamics User's Workshop, Univ. of Tennessee Space Inst. E02-4005-023-84, March 1984.

[16]Baldwin, B. S., and Lomax, H., "Thin Layer Approximation and Algebraic Model for Separated Turbulent Flows," AIAA Paper 78-257, Jan. 1978.